High volumetric and energy densities of methane stored in nanoporous materials at ambient temperatures and moderate pressures

*Nuno Bimbo[1], Andrew J Physick[1], Antonio Noguera-Díaz[1], Adam Pugsley[1], Leighton T Holyfield[1,2], Valeska P Ting[1] and Timothy J Mays[1]**

[1]Department of Chemical Engineering, University of Bath, Claverton Down, Bath, BA2 7AY, United Kingdom

[2]Centre for Doctoral Training in Sustainable Chemical Technologies, University of Bath, Claverton Down, Bath, BA2 7AY, United Kingdom

Keywords: methane adsorption, porous materials, methane storage

Abstract

Experimental results for methane adsorption on two high-surface area carbons (TE7-20 and AX-21) and one metal-organic framework (MIL-101(Cr)) are presented, with isotherms obtained at temperatures ranging from 250 to 350 K and at pressures up to 15 MPa. The isotherms were analysed to determine if these materials could be viable alternatives for on-board solid-state storage of methane. The results show a very high adsorbate density in the pores of all materials, which for some can even exceed liquid methane density. At moderate pressures below 5 MPa, the calculated total energy densities are close to the energy density of methanol, and are almost 40 % of the energy density of gasoline (petrol). Compared with standard compression at the same conditions, the results show that adsorption can be a competitive storage alternative, as it can offer equal volumetric capacities at much lower pressures, hence reducing the energy penalty associated with compression. It is shown that the optimal conditions for adsorptive methane storage in these materials are at moderate pressure ranges, where the gains in amounts stored when using an adsorbent are more pronounced when compared to cylinders of compressed methane gas at the same operating conditions. Finally, a study on deliverable capacities for adsorbed methane was carried out, simulating two charging pressure scenarios of 3.5 and 6.5 MPa and discharge at 0.5 MPa. The results show that some of the tested materials have high working volumetric capacities, with some materials displaying more than 140 kg m^{-3} volumetric working capacity for charging at 6.5 MPa and delivery at 0.5 MPa.

Introduction

The predicted energy demand in the upcoming decades, mostly from less developed parts of the world, will entail a significant strain on primary energy sources worldwide[1, 2]. This has prompted investment in alternative sources of energy, both from governmental and private sources, with renewable sources of energy gaining an increasing share of primary energy conversion[1]. Nowadays, as has been the case for the last two centuries, most of the primary energy comes from fossil fuels, which are finite and will eventually run out. Fossil fuels' popularity is due to their low price and their availability, high volumetric energy content and the ease in converting energy via simple combustion. One interesting and topical fossil fuel is natural gas, which is a mixture whose main component is methane (more than 90 % of its molar composition). While it is hard to dispute that natural gas adds to energy security at a very affordable price in countries like the United States, due to the prospect of exploring shale gas reserves in their continental shelf, increasing methane usage as a strategy for mitigation of greenhouse gas emissions has raised several concerns. Despite methane's combustion emitting less carbon dioxide per unit of energy generated than other fuels (methane has the highest ratio of heat of combustion per carbon atom of any hydrocarbon), methane itself is a very potent greenhouse gas, with a global warming potential of 72 if a 20-year horizon is considered (methane has an atmospheric lifetime of 12.4 years)[3], and increased use will mean more emissions of methane to the atmosphere due to leakages[4]. Leakages are not a trivial matter and can mean that methane has a higher environmental footprint than oil or coal[5] and that its impact in coming decades will be minimal and possibly even negative in climate change[6]. Nonetheless, the exploration and production of natural gas and the prospect of producing shale gas mean that, as has been the case for the last decade, natural gas share in the energy mix has been on the rise and is predicted to continue to grow. This is due to its affordability and availability, and to

the fact that it has many uses, as in electricity production in combined-cycle natural gas turbines, in domestic applications (domestic heating and cooking in developed countries are very reliant on natural gas) and as a commodity in the chemical industry, where it is a precursor to many chemical products.

Another application of methane gas is as an energy fuel in vehicles. Methane is extremely popular in some parts of the world, along with other alternative fuels like Liquefied Petroleum Gas (LPG), to power internal combustion engines. It is a gas at normal pressures and temperatures, so it has poor volumetric density, which is detrimental for on-board storage in vehicles. In addition, methane storage is a relevant issue outside mobile applications, as it is usually obtained from natural gas and transported as LNG at 111 K and atmospheric pressure. This carries some downsides – large tanks are needed to transport LNG (usually a 70 m diameter tank, 45 m high, which can hold 100,000 m^3), which require large and expensive infrastructure[7]. Long term storage is also difficult for LNG, as significant losses occur due to boil-off[7]. Alternatively, natural gas can be compressed at high pressures, with natural gas mixtures rich in ethane and propane compressed at around 12.2 MPa and pure methane gas compressed at twice that pressure (24.4 MPa)[7]. Compression and liquefaction both carry energy penalties and safety issues, so the challenge is to find storage alternatives that are competitive in terms of price and can offer high volumetric densities.

Adsorption of methane in porous materials has been considered as a viable storage alternative precisely because it can increase volumetric densities at moderate conditions[8]. High-surface area materials with porosity in the micropore range can store significant amounts of methane under

moderate pressures[9]. The goal is to keep the energy penalty at a minimum, so adsorptive storage should occur as close to ambient conditions as possible, meaning that it will be above its vapour-liquid critical temperature of 190 K. It has been suggested that high capacities for methane adsorption are a result of a complex interplay of factors, including BET surface areas, enthalpies of adsorption and pore morphologies and distributions[10]. A number of recent reviews highlighted the main materials challenges, which include purity of methane gas, kinetics and enthalpies of the system[11-14]. The kinetics can be an issue since short charging and discharging times are needed. The thermodynamics of the system mean that high enthalpies are beneficial for room temperature methane storage, although they also mean that adsorption of methane will release heat into the system. Adsorption is highly sensitive to temperature, so the thermal management of the storage system becomes an issue. It has been reported that, for storage and delivery of methane at 3 and 0.15 MPa, respectively, the optimum temperature for storage in porous carbons is 254 K and the optimum enthalpy change is 18.8 kJ mol^{-1} [15]. It has also been recently observed that methane adsorbed at high pressures in a zeolite template carbon can have an increasing isosteric enthalpy with coverage[16].

Many adsorbent materials have reported high volumetric and gravimetric methane uptakes at moderate pressures and ambient temperatures. The materials that have showed the highest gravimetric and volumetric uptakes for methane at ambient temperatures and moderate pressures are summarised in Table 1.

Table 1 - Methane gravimetric and volumetric uptakes for different materials. Except where otherwise noted, uptake refers to excess amount.

Material	Volumetric uptake		Gravimetric uptake	Temperature	Pressure	Reference
	kg m^{-3}	cm^3 cm^{-3}	wt. %	K	MPa	
PCN-14	163[a]	230[a]	18.7[a]	290	3.5	[17]
PCN-61	102	145	18.6	298	3.5	[18]
PCN-68	78	99	18.6	298	3.5	[18]
NOTT-109	139[a]	196[a]	17.6[a]	300	3.5	[19]
NU-111	145[a]	205[a]	36.0[a]	298	6.5	[20]
DUT-23 (Co)	107	152	26.8	298	10	[21]
DUT-49	167	236	30.8	298	11	[22]
HKUST-1	160[a]	226[a]	18.4[a]	298	3.5	[23,24]
MOF-210	119[a]	84[a]	47.6[a]	290	3.5	[25]
MIL-101 (Cr)	96	135	21.8	303	6	[26]
AX-21	109[a]	154[a]	22.3[a]	298	3.5	[11]

[a] Calculated total amount

In this work, experimental isotherms measured at temperatures from 250 to 350 K and at pressures up to 15 MPa for the activated carbon AX-21, metal-organic framework MIL-101 (Cr) and activated carbon beads TE7-20 are presented, with the analysis of the results showing high adsorbate densities. The optimum conditions for adsorptive storage and the working capacities for all three materials were also determined.

Experimental and modelling methodology

The materials used in this work are the activated carbon AX-21, the metal-organic framework MIL-101 (Cr) and the activated carbon beads TE7-20. The AX-21 was sourced from Anderson

Company (Anderson Development Company, Inc., Michigan, USA), the MIL-101 (Cr), first reported by Férey et al.[27], was synthesised following a procedure previously reported in Sharpe et al.[28] and adapted from Jiang et al.[29]. The TE7-20 carbon beads were generously provided by MAST Carbon (MAST Carbon International, Basingstoke, UK).

All the samples were characterised using volumetric nitrogen adsorption. A nitrogen isotherm was measured at 77 K up to the vapour pressure (0.1 MPa) on a Micromeritics ASAP 2020 (Micromeritics Instrument Corporation, Georgia, USA). The method used for calculation of BET surface areas was the consistency criteria provided by Rouquerol et al.[30] and the micropore volumes were determined using the Dubinin-Radushkevich (DR) method[31].. Table 2 shows the measured BET surface area, the micropore volumes and the skeletal densities obtained by helium pycnometry for the three materials. To ensure repeatability and reproducibility, different samples of the same batch of material of the MIL-101 (Cr) and the AX-21 and a different batch of TE7 were tested for nitrogen adsorption at 77 K, with the obtained BET surface area measurements shown in Supporting Information. The value obtained for the micropore volume of the AX-21 was 1.97 $cm^3\ g^{-1}$, with other studies reporting a range of similar values, with Carrott et al. citing a value of 1.52 $cm^3\ g^{-1}$ [32], Herrera et al.[33] estimating a value of 1.21 $cm^3\ g^{-1}$ using their proposed method and 1.89 $cm^3\ g^{-1}$ using the conventional method and Mason et al.[11] citing a value of 1.67 $cm^3\ g^{-1}$. The micropore volume obtained for the MIL-101 (Cr) was 0.81 $cm^3\ g^{-1}$. MIL-101 (Cr) is a predominantly mesoporous material, with a pore size distribution, as deduced from its crystal structure, centred around pores of 7, 29 and 34 Å. The 7 Å pore is located in the tetrahedral side pockets, while the 29 and 34 Å mesopores are the cages delimited by 12 Å and 16 x 14.7 Å pentagonal and hexagonal windows, respectively. The total pore volume for our sample was 1.78

$cm^3\ g^{-1}$, as measured by the Horvath-Kawazoe method at 0.99 P/P_0, indicating, as expected, that the majority of porosity of MIL-101 (Cr) is in the mesoporous range. Total pore volumes for the MIL-101 (Cr) range between 1.25 and 2.15 $cm^3\ g^{-1}$ [34]. A powder X-ray diffraction spectrum for the MIL-101 (Cr) tested sample and the pore size distributions for all three materials measured with DFT are in Supporting Information. The value obtained for the TE7-20 for the micropore volume is consistent with some of our previously reported measurements in other samples of MAST carbon beads[35]. The procedure for activating the samples prior to characterisation, thermal analysis, nitrogen isotherms at 77 K, the BET plots, the DR plots for calculating micropore volumes and the pore-size distributions for the AX-21, the MIL-101 (Cr) and the TE7-20, along with the rest of the experimental methodology are in Supporting Information.

Table 2. Characterisation of AX-21, MIL-101 (Cr) and TE7-20. The BET surface areas were determined using the consistency criteria reported by Rouquerol et al.[30] on a nitrogen isotherm at 77 K, the micropore volumes were determined from the nitrogen isotherm at 77 K and the DR method[31] and the skeletal volumes were determined from helium pycnometry on a degassed sample. Quoted uncertainties are standard errors.

Material	AX-21	MIL-101 (Cr)	TE7-20
BET surface area $m^2\ g^{-1}$	2550 ± 30	2520 ± 50	1299 ± 7
Micropore volume $cm^3\ g^{-1}$	1.97 ± 0.01	0.813 ± 0.003	0.520 ± 0.002
Skeletal density $g\ cm^{-3}$	2.67 ± 0.02	1.9 ± 0.3	2.29 ± 0.01

The methane was obtained from a BOC Methane cylinder (BOC Ltd, Surrey, UK. BOC Ltd is now part of The Linde Group) with CP grade of purity (volume fraction of methane of 99.5 %). Methane isotherms were collected at 250, 273, 300, 325 and 350 for the AX-21 and MIL-101 (Cr) and at 273, 300, 325 and 350 K for the TE7-20. The isotherms were collected at each temperature at pressures up to 10 MPa for the MIL-101 (Cr), 13 MPa for the TE7-20 and 15 MPA for the AX-21. This was done as a correction to the isotherms and to obtain the skeletal density for the different materials shown in Table 2. The experimental excess methane isotherms for the AX-21, the MIL-101 (Cr) and the TE7-20 are in Supporting Information.

Results and Discussion

Methane uptake has been traditionally reported as adsorbed volume at standard pressure and temperature, usually in cm^3 (STP) per volume of sample (cm^3 (STP) cm^{-3}) or gravimetrically (cm^3 (STP) g^{-1}). Methane uptakes have also been reported in mmol g^{-1}. In this work, adsorbed quantities are reported as sample-specific weight percent (wt. %), that is per unit mass of degassed adsorbent.

The methane isotherms were modelled using a methodology our group reported in the past, of using excess adsorption data and converting these into an absolute isotherm[36]. More recently, we adapted a model where a distinction is made between excess, absolute and total[28, 37, 38]. The absolute corresponds to the high-density adsorbed phase, with the total corresponding to the total quantity present in the pore, including the gas in the pore space which resembles a bulk gas. Other researchers have also characterised their systems using this approach[11, 39].

The equations that were fit to the isotherms were previously described [28] and they account for excess (eq 1), absolute (eq 2) and total adsorption (eq 3).

$$m_e = \rho_a\, \theta\, V_p - \rho_b \theta\, V_p \leftrightarrow (\rho_a - \rho_b)\, \theta\, V_p \quad (1)$$

$$m_a = m_e + \rho_b\, \theta\, V_p \leftrightarrow \rho_a\, \theta\, V_p \quad (2)$$

$$m_t = m_e + \rho_b V_p \leftrightarrow \rho_a\, \theta\, V_p + \rho_b V_p (1 - \theta) \quad (3)$$

For all equations, m_e is excess adsorption (in our work specified as a percentage of degassed sample weight wt.%), m_a is absolute adsorption (again, converted to wt.%), m_t is total adsorption in wt.%, ρ_a is the density of the adsorbed phase in kg m^{-3}, ρ_b is the density of the bulk phase (kg m^{-3}), θ is the fractional filling of the micropore, and V_p is the micropore volume (which is usually represented in units of cm^{-3} g^{-1}, for consistency in this formula is in units of m^3 kg^{-1}). As in our previous work, excess adsorption is the experimentally obtained value, which corresponds to the Gibbs excess. In our formulae, it is the absolute adsorption minus the bulk amount of the gas that would occupy the same space.

The different isotherms were fit individually following this methodology, using the Tóth equation for the type I isotherm and distinguishing between excess, absolute and total adsorption. The temperature dependence of the parameters was investigated and the only parameter observed to depend on temperature was the affinity parameter b in the Tóth equation, which followed a van't Hoff relation, $b = b_0 \exp(-Q_{st} / RT)$, where b_0 is the pre-exponential or entropic factor, $-Q_{st}$ is the energy or enthalpic factor, and R = 8.314 J K^{-1} mol^{-1} is the molar gas constant. The figures with the individual fittings for all materials and the temperature dependence of the parameters are in Supporting Information. For the analysis, the parameter corresponding to the micropore volume was fixed to the experimental value determined by the DR method. Characterisation using nitrogen

isotherms at 77 K has some inherent issues and it has been shown that argon and CO_2 should also be used for a complete characterisation of porosity of an adsorbent[40], as the accessible surface area depends on the probe molecule used[41]. This has been further confirmed experimentally, when different probe molecules have been used at their normal boiling point to obtain different BET surface areas[42]. Methane has a different size and shape of the probe molecule used for characterisation (which was nitrogen), which could mean that it accesses a different volume. However, the micropore volume obtained from the DR method calculated from the nitrogen isotherm was used. This is justified, as even if the shape of the molecule is different (methane is tetrahedral, nitrogen is linear), the commonly used kinetic molecular diameters are very similar in both, as methane has a 0.380 nm diameter and nitrogen has a 0.364 nm diameter[43]. These kinetic molecular diameters, by Hirschdelfer et al., were obtained by fitting experimental second virial coefficient data to Lennard-Jones parameters and were recently found to be in good agreement with calculated quantum mechanical diameters for both the methane and nitrogen molecules[44].

The density of methane was obtained using data from the Chemistry Webbook from NIST[45], which is based on the REFPROP Fluid Properties Software. This density is calculated using the equation of state for methane provided by Setzmann and Wagner[46], which is the best available equation of state for methane. As in our previous work for hydrogen[36], the equation of state is a complex function to implement, so the densities of methane at different temperatures are fit with a rational function, which is then used to estimate densities at different temperatures. This is detailed in the Supporting Information.

In Figure 1, the excess methane isotherms for the AX-21, the MIL-101 (Cr) and the TE7-20 were fit using a method that distinguishes between excess, absolute and total adsorption and the Tóth equation.

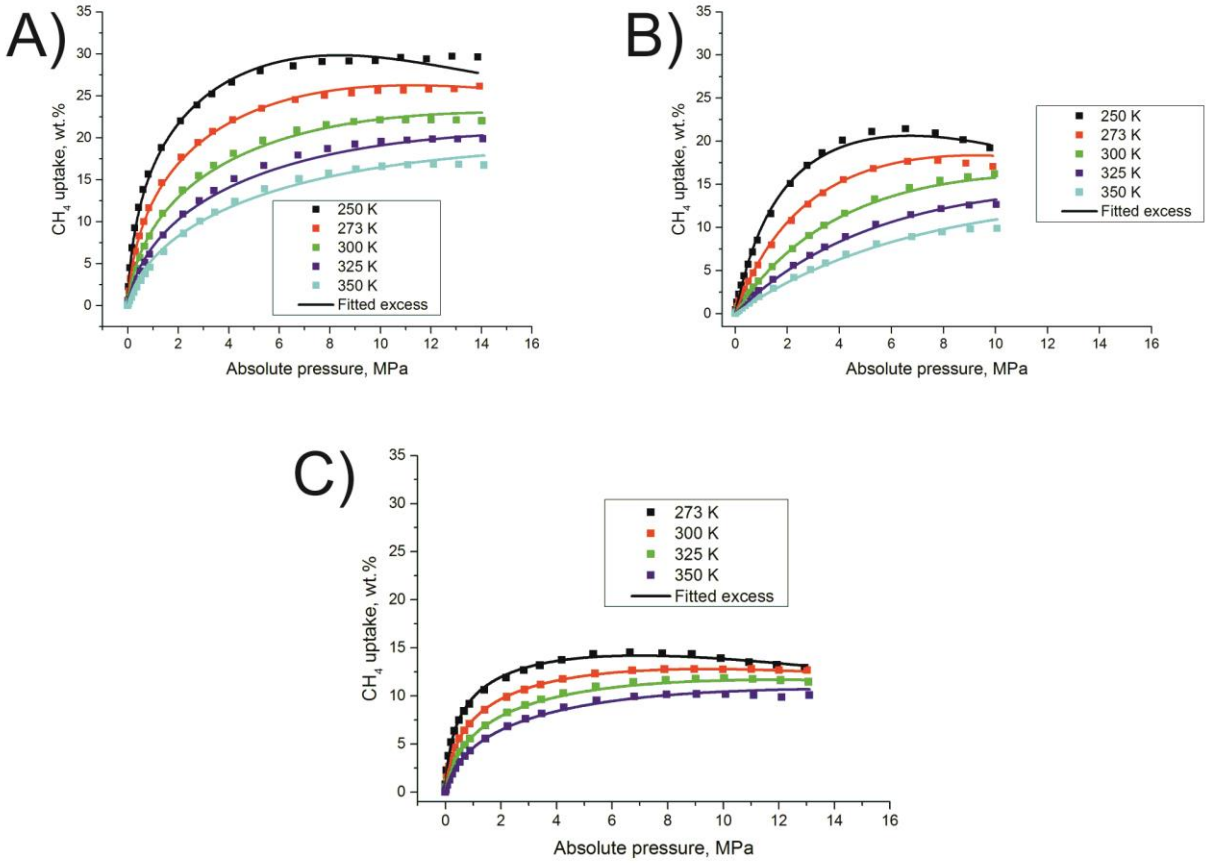

Figure 1. Excess methane isotherms for A) AX-21, B) MIL-101 (Cr) and C) TE7-20. Lines are the best fits to eq 1, squares are the experimental points.

The parameters determined from the fits are in Table 3. The uptakes are reported as a sample-specific percentage of weight (wt. %), dividing the mass of CH_4 by the degassed mass of the sample. The AX-21 has a methane uptake of more than 30 wt. % at 250 K and, at 14 MPa, but the

isotherm shape indicates that it does not seem to have the pores saturated. The MIL-101 (Cr) reaches the maximum excess point[36] around 6 MPa and the excess then starts to diminish. The AX-21 and the MIL-101 (Cr) have almost identical BET surface areas, but, as noted before, the MIL-101 (Cr) is predominantly mesoporous and has a significantly smaller measured micropore volume (the AX-21 has a micropore volume of 1.97 $cm^3\ g^{-1}$, the MIL-101 (Cr) has a micropore volume of 0.81 $cm^3\ g^{-1}$). This difference could explain the notable differences in performance, and evidence points out that large pores do not contribute to the adsorption performance, as, despite offering more free volume for adsorption, the wide pores have a lower energy of interaction [10].

Table 3. Parameters determined from the fitting to the isotherms. The uncertainties are the standard errors from the parameter determination in the non-linear fitting software.

Material	AX-21	MIL-101 (Cr)	TE7-20
Adsorbed density, ρ_a kg m^{-3}	503 ± 12	407 ± 7	462 ± 6
Energy or enthalpic factor, Q_{st} kJ mol^{-1}	15.0 ± 0.2	14.2 ± 0.2	17.8 ± 0.2
Pre-exponential or entropic factor, b_0 MPa^{-1}	1.4 x 10^{-3} ± 1 x 10^{-4}	4.9 x 10^{-4} ± 3 x 10^{-5}	1.5 x 10^{-3} ± 1 x 10^{-4}
Heterogeneity parameter, c -	0.33 ± 0.01	0.99 ± 0.04	0.47 ± 0.01

The adsorbed density parameter shown in Table 3 is considered constant for all temperatures and throughout the pressure range. The assumption of the model is that in the pore the absolute

phase will have a much higher density than the corresponding bulk gas at those conditions and as the pressure increases the volume occupied by the absolute phase will increase. The ratio of volume occupied by this phase and the total pore volume is modelled using a type I equation and in the limit (where the fractional filling of the pore is equal to 1), all the pore is occupied by the absolute phase.

The adsorbed methane density calculated from the fitting of the isotherms shows a very high value for all materials. These values are, for the AX-21 and the TE7-20, in excess of liquid methane density, which is 421 kg m^{-3} at 111 K and atmospheric pressures (0.1 MPa). Moreover, the adsorbate is expected to have some thermal expansion, so the assumption of a constant density throughout the different temperatures means that the adsorbed density is averaged over all the temperatures, so it is expected that it will have a higher value for the lower temperatures. However, as explained in the previous paragraph, these values refer to the density of the absolute phase, which occupies a fraction of the volume in the pore, so the total pore density will only equal that in the limit of the full pore (when the fractional filling is equal to 1). The remaining parameters, Q_{st} and b_0, the enthalpic and entropic factors in the van't Hoff equation, all display values expected for interactions of these materials with methane[16]. The enthalpic contribution in the van't Hoff equation is related to the limiting value at zero coverage for the isosteric enthalpy of adsorption, and it was recently highlighted that an optimum value for the isosteric enthalpies according to the US DOE targets for methane storage would be in the proximity of 20 kJ mol^{-1} [47]. The heterogeneity parameter in the Tóth equation is related to the energetic (structural and chemical) heterogeneity of the surface. It is interesting to note that, for the MIL-101 (Cr), this value is very close to 1, which means an almost homogeneous surface, as a heterogeneity parameter of 1 in the Tóth

equation reduces it to the Langmuir equation. Again, despite the activated carbons being solely composed of carbon and MIL-101 being more heterogeneous in its composition, as it is formed of hydrogen, carbon, chromium, and oxygen atoms, the heterogeneity, as indicated by the fitting of the Tóth equation, shows an almost homogeneous energetic surface for the MIL-101 (Cr). This indicates that for this specific example, chemical heterogeneity is not very important and structural heterogeneity seems to dominate, as the surface of crystalline MIL-101 (Cr) is less structurally diverse than the amorphous carbons. This is also an important factor to take into account in methane adsorption, as, according to Bhatia and Myers, the presence of heterogeneity in the surfaces is detrimental for methane storage[15].

The value obtained for the adsorbed density is not a true measure of the amount contained in the pores of a material at moderate pressures, as the pore might only be completely saturated at extremely high pressures. The total density in the pore (total amount divided by the experimental micropore volume) was plotted as a function of the pressure for all three materials and compared with the adsorbed density parameter and the liquid density of methane at 111 K and 0.1 MPa, based on total adsorption, which accounts for absolute and the gas at bulk conditions contained in the pore. In Figure 2, the densities in the micropores as a function of pressure at 250, 273, 300, 325 and 350 K and up to 20 MPa, based on the parameters shown in Table 3, are shown for the AX-21, the MIL-101 (Cr) and the TE7-20.

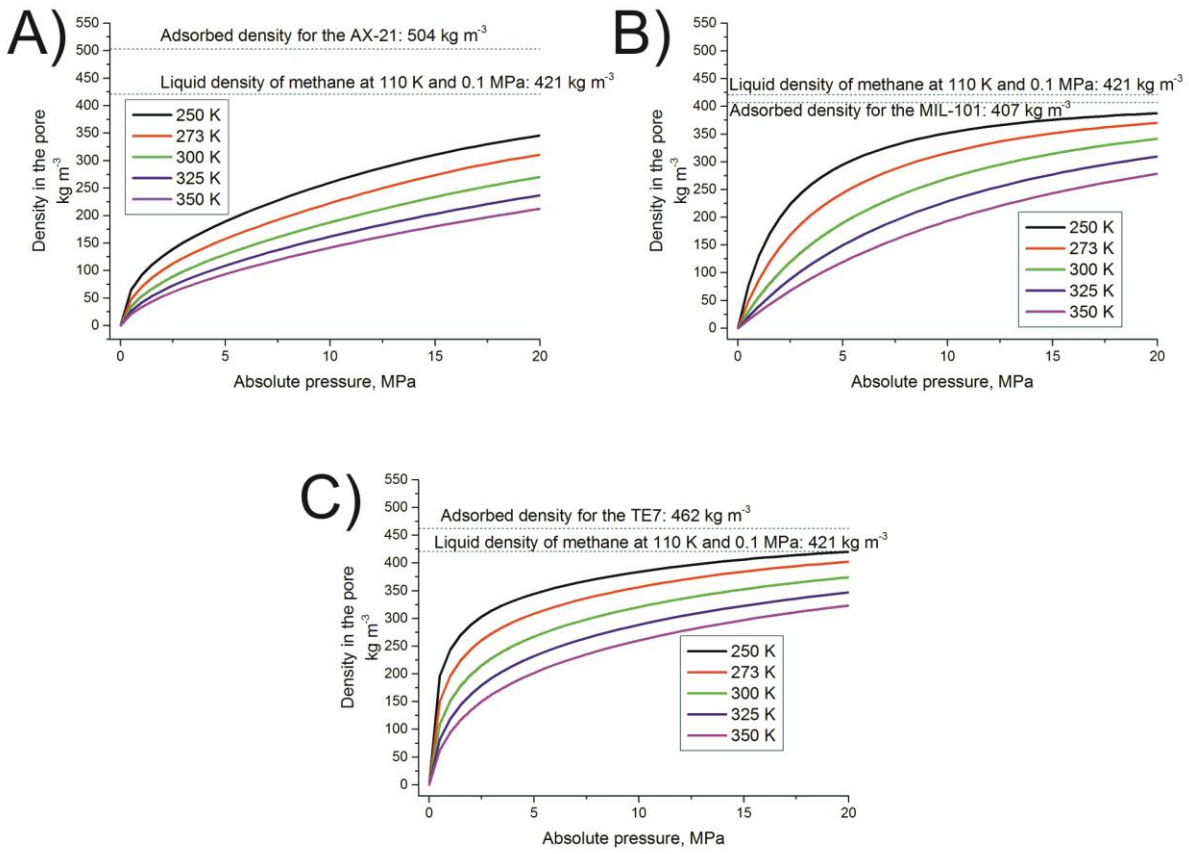

Figure 2. Adsorbed density of methane isotherms for A) AX-21, B) MIL-101 (Cr) and C) TE7-20 determined from the parameters in Table 3, from 250 to 350 K and up to 20 MPa compared with the adsorbed density and the density of liquid methane at 111 K and 0.1 MPa (dashed horizontal lines).

For both the MIL-101 (Cr) and the TE7-20, the densities determined from total adsorption can reach values in the vicinity of 400 kg m^{-3} at 273 K and 20 MPa. These densities for methane are higher than the ones seen in a recent work with computer simulations for various diameters of carbon nanotubes[48] and also higher than the ones determined by Rodríguez-Reinoso et al.[49], with the former study calculating densities of 200 kg m^{-3} and the latter reporting limiting densities of

230 kg m^{-3}. However, even when just using the maximum excess uptake for the MIL-101 (Cr) at 250 K, which is 22.5 wt. %, the obtained density using an experimental pore volume of 0.81 cm^3 g^{-1} can exceed 270 kg m^{-3}. Bénard and Chahine also modelled high-pressure adsorption isotherms of methane on activated carbon and observed that the whole temperature range could be fitted if a constant density at a maximum capacity of 26.5 mol dm^{-3} (which corresponds to 425 kg m^{-3}) was used[50]. This value is very close to the ones observed in this work.

The next step in the analysis was to estimate system capacities and obtain volumetric densities for whole cylinders, taking into account other material properties, like skeletal densities and available micropore volumes. The skeletal densities and micropore volumes used were the ones determined experimentally and shown in Table 2. The methodology for this analysis was presented before[38], where the total adsorption was used to estimate the amount of gas present in a cylinder occupied by the adsorbent. The packing factor and filling factor were both considered equal to 1. The energy densities on the right-hand side axis in Figure 3 were obtained using the enthalpy of combustion of methane, which is 55.47 MJ kg^{-1} (890 kJ mol^{-1})[51]. For comparison, the volumetric densities obtained from compression of methane in an empty cylinder at the same temperatures are also shown (dashed lines).

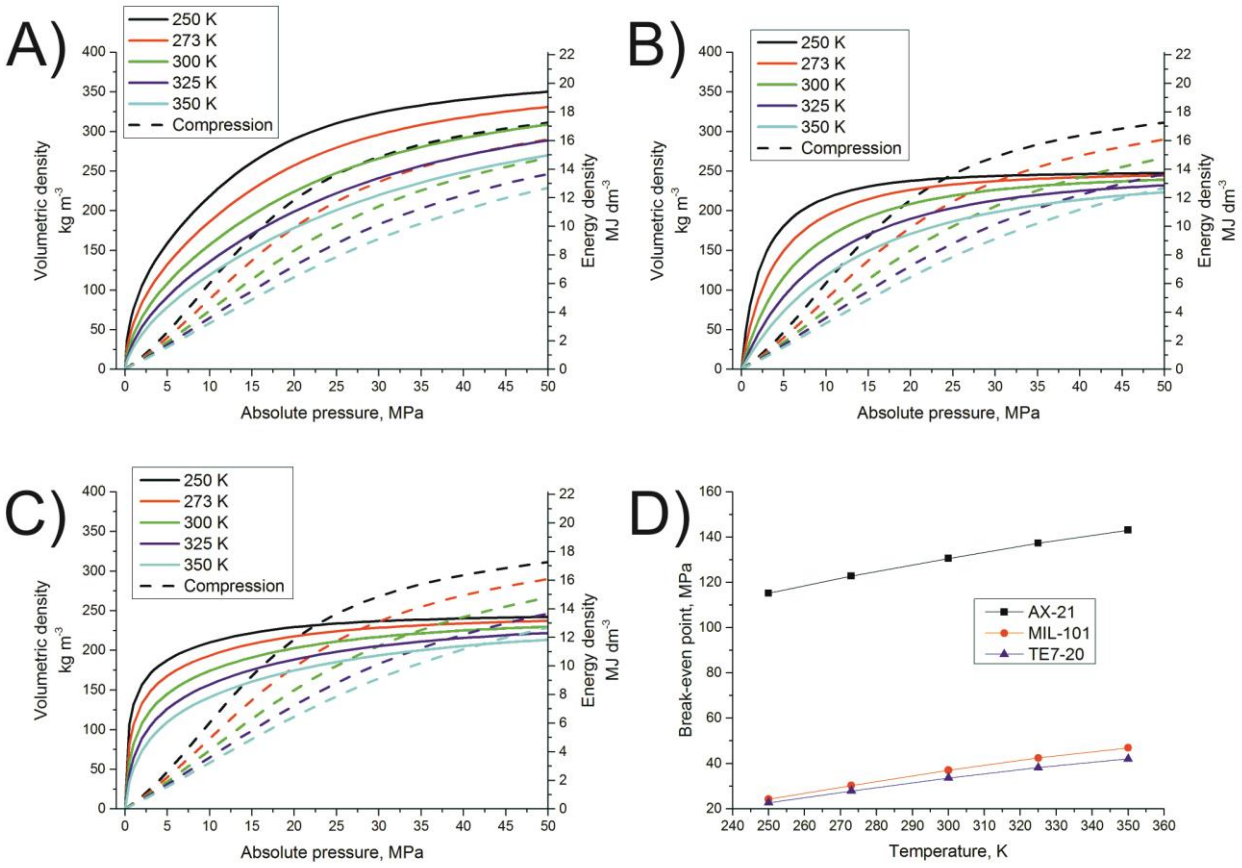

Figure 3. The amounts stored by adsorption (solid lines) compared with the amounts stored by compression (dashed lines), with the break-even points, from 250 to 350 K and up to 30 MPa. The materials shown are A) AX-21, B) MIL-101 (Cr) and C) TE7-20. The break-even pressures as a function of temperature for each material are shown in D).

In Figure 3, the methane volumetric densities using adsorption and compression, from 250 to 350 K and up to 50 MPa, for the AX-21, the MIL-101 (Cr) and the TE7-20, are shown. The figures show many interesting features. The first interesting feature is the break-even point – for the three materials shown, adsorption has higher volumetric densities at moderate pressures but with increasing pressure a pressure is reached (the break-even pressure) where compression has higher volumetric methane densities than adsorption[38, 52, 53]. This is due to the solid adsorbent displacing

a volume in the cylinder and, at certain operating conditions, the volumetric enhancement due to adsorption does not compensate for the volumes the adsorbent displaces. As shown in the past[38, 52], the break-even pressure is temperature and material-dependent but it does not depend on how much adsorbent is present in a given volume and will be the same for the same conditions, regardless of the volume fraction occupied by the adsorbent in the tank. Figure 3 also shows that all of the materials exhibit an increasing break-even pressure with temperature, and the AX-21 has a break-even pressure of more than 110 MPa for all the measured temperatures. This is due to the large micropore volume available and the fact that, as it can be seen in Figure 3, high pressures are needed for saturation in the micropores of AX-21, which are probably due to its high measured micropore volume (1.96 $cm^3\ g^{-1}$).

Another interesting feature in Figure 3 is the values of the volumetric densities and the corresponding energy densities. According to our analysis, the AX-21, the MIL-101 (Cr) and the TE7-20 all reach a volumetric density of 230 kg m^{-3}, at 250 K at 11, 15 and 32 MPa, respectively. This volumetric density corresponds to an energy density of 12.8 MJ dm^{-3}, which is very close to energy density of methanol (15.6 MJ dm^{-3}), and close to 40 % of the energy density contained in petrol (34.2 MJ dm^{-3}), for adsorbed methane at moderate pressures and ambient temperatures. According to this analysis, the TE7 and the MIL-101 at 250 K would meet the US DOE targets for natural gas storage, which consist of meeting the energy density of compressed natural gas (9.2 MJ dm^{-3}) at pressures below 3.5 MPa[54]. Wilmer et al.[55] screened more than 130,000 metal-organic frameworks and found 300 hypothetical structures could outperform this target at 298 K and 3.5 MPa. While the MIL-101 (Cr) and the TE7-20 seem to saturate their uptakes at pressures close to 20 MPa, where they reach a capacity just under 250 kg m^{-3}, the AX-21 volumetric density can go

as high as 350 kg m^{-3} at 50 MPa, and the shape of the total isotherm indicates that it is not saturated at those pressures.

As seen in Figure 3, there is a break-even pressure for all materials, but the optimal point has to be in conditions where there is a bigger gain from an adsorbent, as the adsorbent adds additional weight to the cylinders. In Figure 4, a comparison of volumetric methane densities and energy densities for the AX-21, the MIL-101 (Cr) and the TE7-20, from 250 to 350 K and up to 50 MPa, is made.

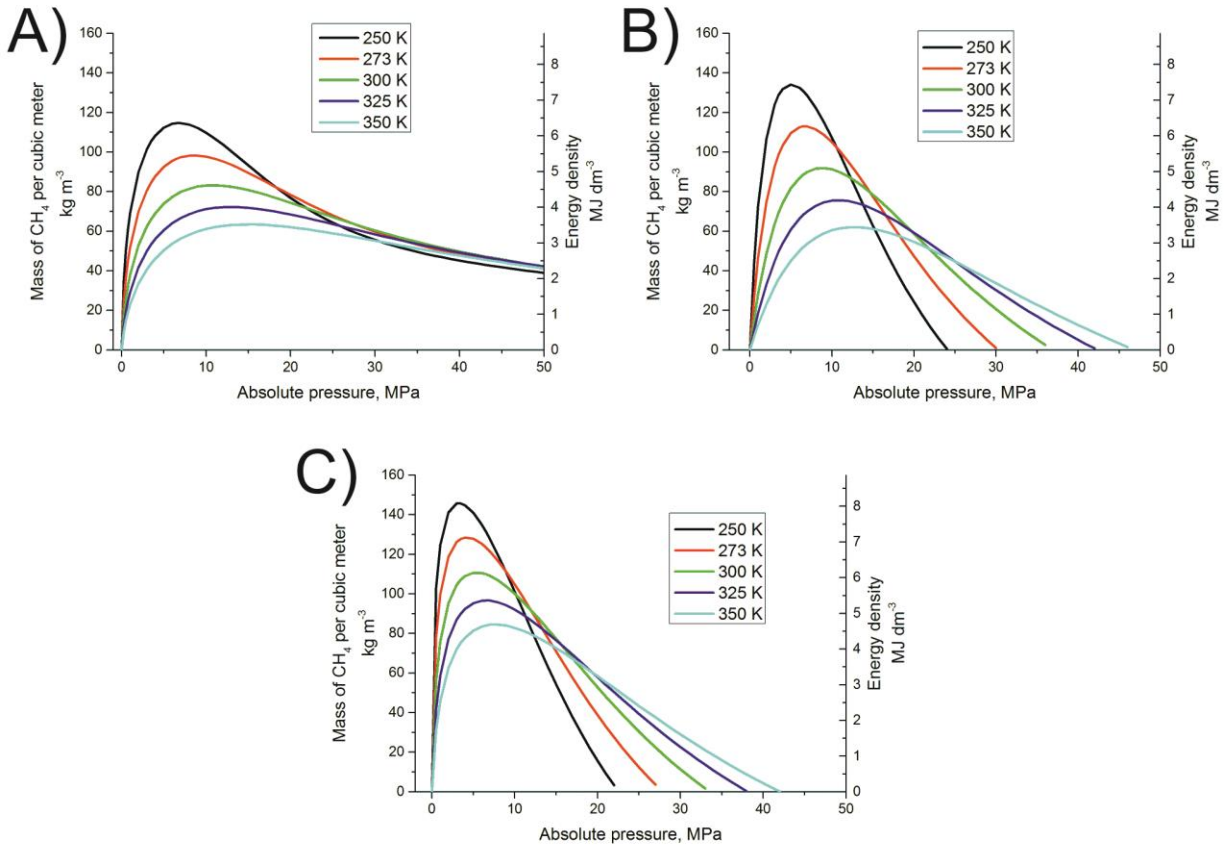

Figure 4. Gains in volumetric density and energy density by using adsorption over compression at the same pressures and temperatures, from 250 to 350 K and up to 30 MPa. The materials shown are A) AX-21, B) MIL-101 (Cr) and C) TE7-20.

As it can be seen from Figure 4, the maximum gain in using an adsorbent varies with material, but it is situated around 5 MPa for all materials. As evident in Figure 4, adsorptive storage of methane in the pressure ranges above 15 MPa for the MIL-101 (Cr) and the AX-21 and above 10 MPa for the TE7-20, is detrimental to the use of adsorbents, as the gains over an empty cylinder at equal conditions are residual. The MIL-101 (Cr) and TE7-20 peak at pressures around 5 MPa and then have a sharp drop in gains over compression, as their pores quickly fill up and increased pressure will only increase the density of the bulk. The AX-21 also shows a peak around 5 MPa but there is still gain at 50 MPa, which will be positive until the break-even pressure, which, as shown in Figure 3, is over 110 MPa. The overall gain of using adsorbents in cylinders, as shown in all materials, can be as high as 140 kg m^{-3} in volumetric densities, for 250 K and at pressures of less than 5 MPa. The volumetric density of methane at 5 MPa and 250 K is close to 46 kg m^{-3}, so adding one of these adsorbents represents an additional 90 kg of methane stored for every cubic meter at these conditions.

The last step of the analysis deals with the working capacities of methane in these materials. Using vacuum to fully desorb methane is costly to operate and potentially difficult to implement in practical applications, so a higher discharge pressure has to be considered[56]. The working capacities were calculated for two different scenarios, with charging pressures of 3.5 and of 6.5 MPa. For both cases, the total amount was used, which is the one that represents the total amount of methane contained in the material, and the delivery pressure fixed at 0.5 MPa. Other reports have used similar charging and delivery pressures[47, 56-58]. The baseline scenario, which is charging

and discharging at those pressures in an empty cylinder, is also presented for comparison. In Figure 5, the working capacities for the AX-21, the MIL-101 (Cr) and the TE7-20 are presented.

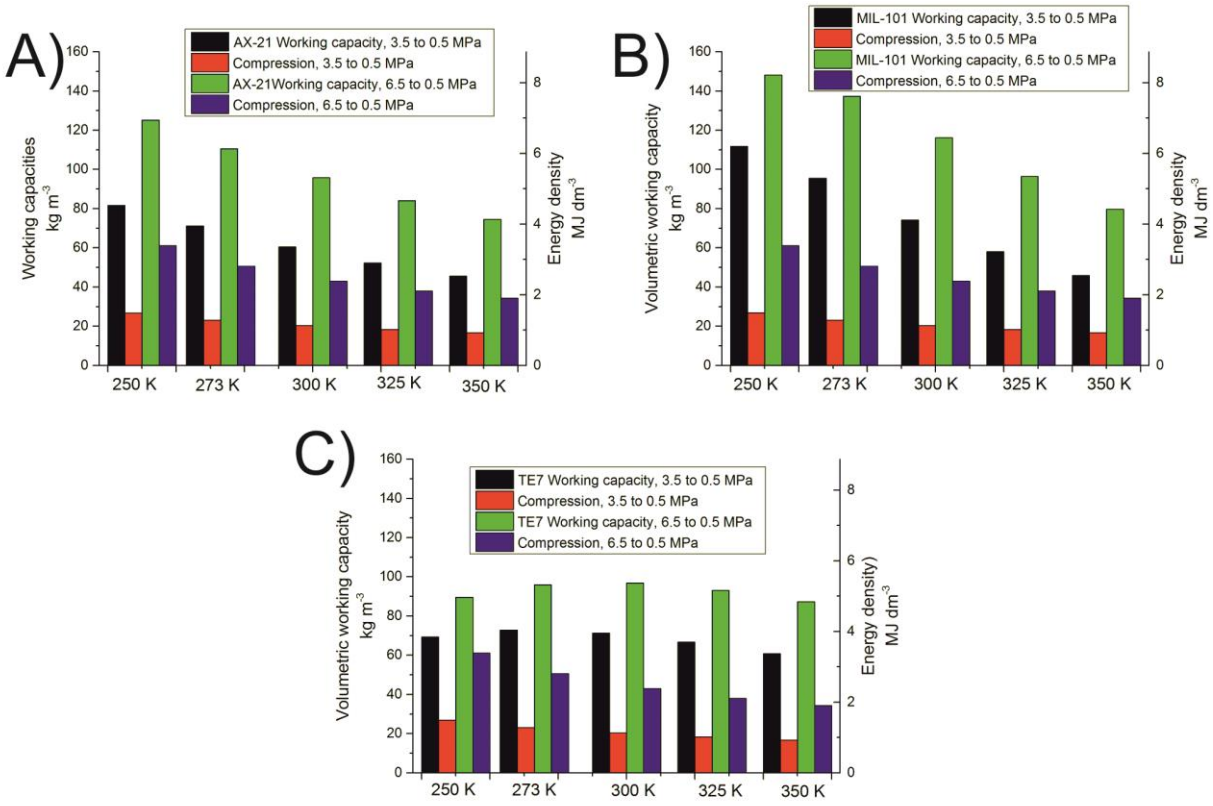

Figure 5. The working capacities for A) AX-21, B) MIL-101 (Cr) and C) TE7-20 from 250 to 350 K. The working capacities are calculated for two scenarios – charging at 3.5 and 6.5 MPa, delivery at 0.5 MPa. A comparison with compression in the same conditions is shown for every material.

The working capacities show high volumetric densities for all of the materials, with the MIL-101 (Cr) showing a working capacity of 140 kg m^{-3} for charging at 6.5 MPa and discharging at 0.5 MPa at 250 K. Even for the different scenario of charging at 3.5 MPa, the MIL-101 (Cr) has working capacity of more than 100 kg m^{-3} at 250 K, which compares to a working capacity of

30 kg m^{-3} for the empty cylinder case. MIL-101 (Cr) has lower methane uptakes than AX-21 and lower volumetric and energy densities than AX-21, but both MIL-101 (Cr) and TE7-20 show a high adsorbed density at moderate pressures. This influences the working capacities, as the differences between the total amounts at 0.5 and 3.5 or 6.5 MPa on the MIL-101 (Cr) outperform those of the AX-21. The AX-21, despite showing high volumetric densities, is not fully saturated, even at 50 MPa, as seen in Figure 3. The difference in total amounts stored in the two materials in the moderate pressure range (3.5 or 6.5 MPa) explain why, regardless of adsorbing more and of showing a higher volumetric density, the AX-21 has a lower working capacity than the MIL-101 (Cr). For the TE7-20, the working capacities increase from 250 to 273 K and then slightly decrease with temperature. The amounts in a container full of adsorbent at 6.5, 3.5 and 0.5 MPa diminish as temperature increases, as would be expected, since lower temperatures correspond to a higher energy of interaction for adsorption. However, in this case, the shape of the isotherm, which is steep at lower pressures for the TE7-20 and levels off at higher pressures, means that the working capacities actually increase at the first temperature (*i.e.* the difference between total amount adsorbed at 6.5 and 0.5 MPa at 273 K is larger than at 250 K). While not observed for the other two materials and not very common, this feature should not be surprising. As would be expected, the working capacity is very sensitive to temperature, and at higher temperatures the added gains of using adsorbents for adsorptive storage will be mitigated.

Conclusions

Although methane adsorption in porous materials has been studied for a long time, recent developments that include new sources of methane and the considerable developments in adsorbent materials have put adsorptive methane storage for vehicular transport on the agenda

again. The porous materials outlook has also considerably changed recently, with the emergence of thousands of new tailored porous materials with enhanced properties that can be suitable for solid-state methane storage. The analysis presented here shows that, using a methodology reported in the past for supercritical hydrogen storage, adsorbed methane can be a competitive alternative for storage, as some materials can offer high volumetric methane densities and high energy densities at moderate pressures and ambient temperatures. The results show that methane can have high average adsorbed densities in the pore, which can approach or even exceed the density of liquid methane at its normal boiling point. Densities approaching liquid methane density at its normal boiling point might only be reached when the pore is saturated with methane, but the results also show that high average adsorbed densities are within reach, at moderate pressures and ambient temperatures. When doing a system analysis and simulating materials in cylinders, it is shown that adsorbed methane can have an energy density close to that of methanol and about 40 % of the energy density of gasoline (petrol). A comparison between compression and adsorption at the same conditions also show the benefits of adding an adsorbent in a cylinder, as it adds a considerable additional amount stored over compression at moderate ranges. Finally, the working capacities under two different scenarios – charging at 3.5 and 6.5 MPa – also show the high potential working capacities, even with a delivery pressure of 0.5 MPa, for all three materials.

Supporting Information

The experimental methodology, including the synthesis and sourcing of materials, the activation of the samples prior to characterization and sorption measurements, the excess methane isotherms, the analysis of kinetic data and standard deviations, thermal analysis, nitrogen isotherms at 77 K,

BET plots, DR plots, pore-size distributions, individual isothermal fits and temperature dependence of the parameters are in Supporting Information.

Corresponding author:

*Dr Timothy J Mays – Department of Chemical Engineering, 9 W Building, University of Bath, Claverton Down, BA2 7AY, United Kingdom. Email – T.J.Mays@bath.ac.uk

Acknowledgements

The authors would like to thank Dr Darren Broom for helpful comments. NB and TJM gratefully acknowledge support from the UK Engineering and Physical Sciences Research Council (EPSRC), especially H2FC SUPERGEN grants EP/K021109/1 and EP/J016454/1. AJP is supported by an EPSRC DTA studentship. AND and LTH thank the University of Bath for URS studentships and LTH also thanks the Centre for Doctoral Training in Sustainable Chemical Technologies (EPSRC grant EP/L016354/1) for financial support. VPT thanks the University of Bath for a Prize Research Fellowship. The authors thank MAST Carbon International UK for providing the TE7-20 carbon beads.

References

1. *World Energy Outlook 2010,* International Energy Agency, 2010
2. *Annual Energy Outlook 2014,* US Energy Information Administration, 2014
3. IPCC, *Climate Change 2013: The Physical Science Basis. Contribution of Working Group I to the Fifth Assessment Report of the Intergovernmental Panel on Climate Change*. Cambridge, United Kingdom and New York, NY, USA, 2013.
4. Brandt, A. R.; Heath, G. A.; Kort, E. A.; O'Sullivan, F.; Petron, G.; Jordaan, S. M.; Tans, P.; Wilcox, J.; Gopstein, A. M.; Arent, D.; Wofsy, S.; Brown, N. J.; Bradley, R.; Stucky, G. D.;

Eardley, D.; Harriss, R., Methane Leaks from North American Natural Gas Systems. *Science*, **2014,** 343, (6172), 733-735.
5. Howarth, R. W.; Ingraffea, A.; Engelder, T., Natural gas: Should fracking stop? *Nature*, **2011,** 477, (7364), 271-275.
6. McJeon, H.; Edmonds, J.; Bauer, N.; Clarke, L.; Fisher, B.; Flannery, B. P.; Hilaire, J.; Krey, V.; Marangoni, G.; Mi, R.; Riahi, K.; Rogner, H.; Tavoni, M., Limited impact on decadal-scale climate change from increased use of natural gas. *Nature*, **2014,** 514, (7523), 482-485.
7. Mokhatab, S.; Poe, W. A.; Speight, J. G., *Handbook of natural gas transmission and processing*. Gulf Professional Pub.: Burlington, MA, 2006.
8. Menon, V. C.; Komarneni, S., Porous adsorbents for vehicular natural gas storage: A review. *J Porous Mat*, **1998,** 5, (1), 43-58.
9. Fernandez, M.; Woo, T. K.; Wilmer, C. E.; Snurr, R. Q., Large-Scale Quantitative Structure-Property Relationship (QSPR) Analysis of Methane Storage in Metal-Organic Frameworks. *J Phys Chem C*, **2013,** 117, (15), 7681-7689.
10. Duren, T.; Sarkisov, L.; Yaghi, O. M.; Snurr, R. Q., Design of new materials for methane storage. *Langmuir*, **2004,** 20, (7), 2683-2689.
11. Mason, J. A.; Veenstra, M.; Long, J. R., Evaluating metal-organic frameworks for natural gas storage. *Chem Sci*, **2014,** 5, (1), 32-51.
12. Makal, T. A.; Li, J. R.; Lu, W. G.; Zhou, H. C., Methane storage in advanced porous materials. *Chem Soc Rev*, **2012,** 41, (23), 7761-7779.
13. Konstas, K.; Osl, T.; Yang, Y. X.; Batten, M.; Burke, N.; Hill, A. J.; Hill, M. R., Methane storage in metal organic frameworks. *J Mater Chem*, **2012,** 22, (33), 16698-16708.
14. He, Y. B.; Zhou, W.; Qian, G. D.; Chen, B. L., Methane storage in metal-organic frameworks. *Chem Soc Rev*, **2014,** 43, (16), 5657-5678.
15. Bhatia, S. K.; Myers, A. L., Optimum conditions for adsorptive storage. *Langmuir*, **2006,** 22, (4), 1688-1700.
16. Stadie, N. P.; Murialdo, M.; Ahn, C. C.; Fultz, B., Anomalous Isosteric Enthalpy of Adsorption of Methane on Zeolite-Templated Carbon. *J Am Chem Soc*, **2013,** 135, (3), 990-993.
17. Ma, S. Q.; Sun, D. F.; Simmons, J. M.; Collier, C. D.; Yuan, D. Q.; Zhou, H. C., Metal-organic framework from an anthracene derivative containing nanoscopic cages exhibiting high methane uptake. *J Am Chem Soc*, **2008,** 130, (3), 1012-1016.
18. Yuan, D. Q.; Zhao, D.; Sun, D. F.; Zhou, H. C., An Isoreticular Series of Metal-Organic Frameworks with Dendritic Hexacarboxylate Ligands and Exceptionally High Gas-Uptake Capacity. *Angew Chem Int Edit*, **2010,** 49, (31), 5357-5361.
19. He, Y. B.; Zhou, W.; Yildirim, T.; Chen, B. L., A series of metal-organic frameworks with high methane uptake and an empirical equation for predicting methane storage capacity. *Energ Environ Sci*, **2013,** 6, (9), 2735-2744.
20. Peng, Y.; Srinivas, G.; Wilmer, C. E.; Eryazici, I.; Snurr, R. Q.; Hupp, J. T.; Yildirim, T.; Farha, O. K., Simultaneously high gravimetric and volumetric methane uptake characteristics of the metal-organic framework NU-111. *Chem Commun*, **2013,** 49, (29), 2992-2994.
21. Klein, N.; Senkovska, I.; Baburin, I. A.; Grunker, R.; Stoeck, U.; Schlichtenmayer, M.; Streppel, B.; Mueller, U.; Leoni, S.; Hirscher, M.; Kaskel, S., Route to a Family of Robust, Non-interpenetrated Metal-Organic Frameworks with pto-like Topology. *Chem-Eur J*, **2011,** 17, (46), 13007-13016.

22. Stoeck, U.; Krause, S.; Bon, V.; Senkovska, I.; Kaskel, S., A highly porous metal-organic framework, constructed from a cuboctahedral super-molecular building block, with exceptionally high methane uptake. *Chem Commun*, **2012,** 48, (88), 10841-10843.
23. Chui, S. S. Y.; Lo, S. M. F.; Charmant, J. P. H.; Orpen, A. G.; Williams, I. D., A chemically functionalizable nanoporous material [Cu-3(TMA)(2)(H2O)(3)](n). *Science*, **1999,** 283, (5405), 1148-1150.
24. Zhou, W., Methane Storage in Porous Metal-Organic Frameworks: Current Records and Future Perspectives. *Chem Rec*, **2010,** 10, (3), 200-204.
25. Furukawa, H.; Ko, N.; Go, Y. B.; Aratani, N.; Choi, S. B.; Choi, E.; Yazaydin, A. O.; Snurr, R. Q.; O'Keeffe, M.; Kim, J.; Yaghi, O. M., Ultrahigh Porosity in Metal-Organic Frameworks. *Science*, **2010,** 329, (5990), 424-428.
26. Llewellyn, P. L.; Bourrelly, S.; Serre, C.; Vimont, A.; Daturi, M.; Hamon, L.; De Weireld, G.; Chang, J. S.; Hong, D. Y.; Hwang, Y. K.; Jhung, S. H.; Ferey, G., High uptakes of CO2 and CH4 in mesoporous metal-organic frameworks MIL-100 and MIL-101. *Langmuir*, **2008,** 24, (14), 7245-7250.
27. Ferey, G.; Mellot-Draznieks, C.; Serre, C.; Millange, F.; Dutour, J.; Surble, S.; Margiolaki, I., A chromium terephthalate-based solid with unusually large pore volumes and surface area. *Science*, **2005,** 309, (5743), 2040-2042.
28. Sharpe, J. E.; Bimbo, N.; Ting, V. P.; Burrows, A. D.; Jiang, D. M.; Mays, T. J., Supercritical hydrogen adsorption in nanostructured solids with hydrogen density variation in pores. *Adsorption*, **2013,** 19, (2-4), 643-652.
29. Jiang, D. M.; Burrows, A. D.; Edler, K. J., Size-controlled synthesis of MIL-101(Cr) nanoparticles with enhanced selectivity for CO2 over N-2. *Crystengcomm*, **2011,** 13, (23), 6916-6919.
30. Rouquerol, J.; Llewellyn, P.; Rouquerol, F., Is the BET equation applicable to microporous adsorbents? *Stud Surf Sci Catal*, **2006,** 160, 49-56.
31. Dubinin, M. M.; Zaverina, E. D.; Radushkevich, L. V., Sorbtsiya I Struktura Aktivnykh Uglei .1. Issledovanie Adsorbtsii Organicheskikh Parov. *Zh Fiz Khim*, **1947,** 21, (11), 1351-1362.
32. Carrott, P. J. M.; Roberts, R. A.; Sing, K. S. W., Adsorption of Nitrogen by Porous and Nonporous Carbons. *Carbon*, **1987,** 25, (1), 59-68.
33. Herrera, L. F.; Fan, C. Y.; Nguyen, V.; Do, D. D.; Horikawa, T.; Nicholson, D., A self-consistent method to determine accessible volume, area and pore size distribution (APSD) of BPL, Norit and AX-21 activated carbon. *Carbon*, **2012,** 50, (2), 500-509.
34. Chowdhury, P.; Bikkina, C.; Gumma, S., Gas Adsorption Properties of the Chromium-Based Metal Organic Framework MIL-101. *J Phys Chem C*, **2009,** 113, (16), 6616-6621.
35. Hruzewicz-Kolodziejczyk, A.; Ting, V. P.; Bimbo, N.; Mays, T. J., Improving comparability of hydrogen storage capacities of nanoporous materials. *Int J Hydrogen Energ*, **2012,** 37, (3), 2728-2736.
36. Bimbo, N.; Ting, V. P.; Hruzewicz-Kolodziejczyk, A.; Mays, T. J., Analysis of hydrogen storage in nanoporous materials for low carbon energy applications. *Faraday Discuss*, **2011,** 151, 59-74.
37. Bimbo, N.; Sharpe, J. E.; Ting, V. P.; Noguera-Diaz, A.; Mays, T. J., Isosteric enthalpies for hydrogen adsorbed on nanoporous materials at high pressures. *Adsorption*, **2014,** 20, (2-3), 373-384.

38. Sharpe, J. E.; Bimbo, N.; Ting, V. P.; Rechain, B.; Joubert, E.; Mays, T. J., Modelling the potential of adsorbed hydrogen for use in aviation (accepted). *Micropor Mesopor Mat*, **2014**, (Special Edition - COPS - X).
39. Schlichtenmayer, M.; Hirscher, M., Nanosponges for hydrogen storage. **2012,** 22, (20), 10134-10143.
40. Silvestre-Albero, J.; Silvestre-Albero, A.; Rodríguez-Reinoso, F.; Thommes, M., Physical characterization of activated carbons with narrow microporosity by nitrogen (77.4 K), carbon dioxide (273 K) and argon (87.3 K) adsorption in combination with immersion calorimetry. **2012,** 50, (9), 3128-3133.
41. Duren, T.; Millange, F.; Ferey, G.; Walton, K. S.; Snurr, R. Q., Calculating geometric surface areas as a characterization tool for metal-organic frameworks. *J Phys Chem C*, **2007,** 111, (42), 15350-15356.
42. Streppel, B.; Hirscher, M., BET specific surface area and pore structure of MOFs determined by hydrogen adsorption at 20 K. *Phys Chem Chem Phys*, **2011,** 13, (8), 3220-3222.
43. Hirschfelder, J. O.; Curtiss, C. F.; Bird, R. B.; University of Wisconsin. Theoretical Chemistry Laboratory., *Molecular theory of gases and liquids*. Corrected printing with notes added. ed.; Wiley: New York, 1965.
44. Mehio, N.; Dai, S.; Jiang, D. E., Quantum Mechanical Basis for Kinetic Diameters of Small Gaseous Molecules. *J Phys Chem A*, **2014,** 118, (6), 1150-1154.
45. NIST, NIST Chemistry WebBook. http://webbook.nist.gov/chemistry/ (accessed 12 November 2014),
46. Setzmann, U.; Wagner, W., A New Equation of State and Tables of Thermodynamic Properties for Methane Covering the Range from the Melting Line to 625-K at Pressures up to 1000-Mpa. *J Phys Chem Ref Data*, **1991,** 20, (6), 1061-1155.
47. Lee, S. J.; Bae, Y. S., Can Metal-Organic Frameworks Attain New DOE Targets for On-Board Methane Storage by Increasing Methane Heat of Adsorption? *J Phys Chem C*, **2014,** 118, (34), 19833-19841.
48. Zhu, X. Y.; Zhao, Y. P., Atomic Mechanisms and Equation of State of Methane Adsorption in Carbon Nanopores. *J Phys Chem C*, **2014,** 118, (31), 17737-17744.
49. Rodriguez-Reinoso, F.; Almansa, C.; Molina-Sabio, M., Contribution to the evaluation of density of methane adsorbed on activated carbon. *J Phys Chem B*, **2005,** 109, (43), 20227-20231.
50. Benard, P.; Chahine, R., Modeling of high-pressure adsorption isotherms above the critical temperature on microporous adsorbents: Application to methane. *Langmuir*, **1997,** 13, (4), 808-813.
51. Atkins, P. W.; De Paula, J., *Atkins' Physical chemistry*. Oxford University Press: Oxford ; New York, 2006.
52. Bimbo, N.; Ting, V. P.; Sharpe, J. E.; Mays, T. J., Analysis of optimal conditions for adsorptive hydrogen storage in microporous solids. *Colloid Surface A*, **2013,** 437, 113-119.
53. Hardy, B.; Corgnale, C.; Chahine, R.; Richard, M. A.; Garrison, S.; Tamburello, D.; Cossement, D.; Anton, D., Modeling of adsorbent based hydrogen storage systems. *Int J Hydrogen Energ*, **2012,** 37, (7), 5691-5705.
54. ARPA-e, Methane Opportunities for Vehicular Energy (MOVE). (https://arpa-e-foa.energy.gov/ (accessed 24 November 2014),
55. Wilmer, C. E.; Leaf, M.; Lee, C. Y.; Farha, O. K.; Hauser, B. G.; Hupp, J. T.; Snurr, R. Q., Large-scale screening of hypothetical metal-organic frameworks. *Nat Chem*, **2012,** 4, (2), 83-89.

56. Gandara, F.; Furukawa, H.; Lee, S.; Yaghi, O. M., High Methane Storage Capacity in Aluminum Metal-Organic Frameworks. *J Am Chem Soc*, **2014,** 136, (14), 5271-5274.
57. Li, B.; Wen, H. M.; Wang, H. L.; Wu, H.; Tyagi, M.; Yildirim, T.; Zhou, W.; Chen, B. L., A Porous Metal-Organic Framework with Dynamic Pyrimidine Groups Exhibiting Record High Methane Storage Working Capacity. *J Am Chem Soc*, **2014,** 136, (17), 6207-6210.
58. Rana, M. K.; Koh, H. S.; Zuberi, H.; Siegel, D. J., Methane Storage in Metal-Substituted Metal-Organic Frameworks: Thermodynamics, Usable Capacity, and the Impact of Enhanced Binding Sites. *J Phys Chem C*, **2014,** 118, (6), 2929-2942.

TOC graphic

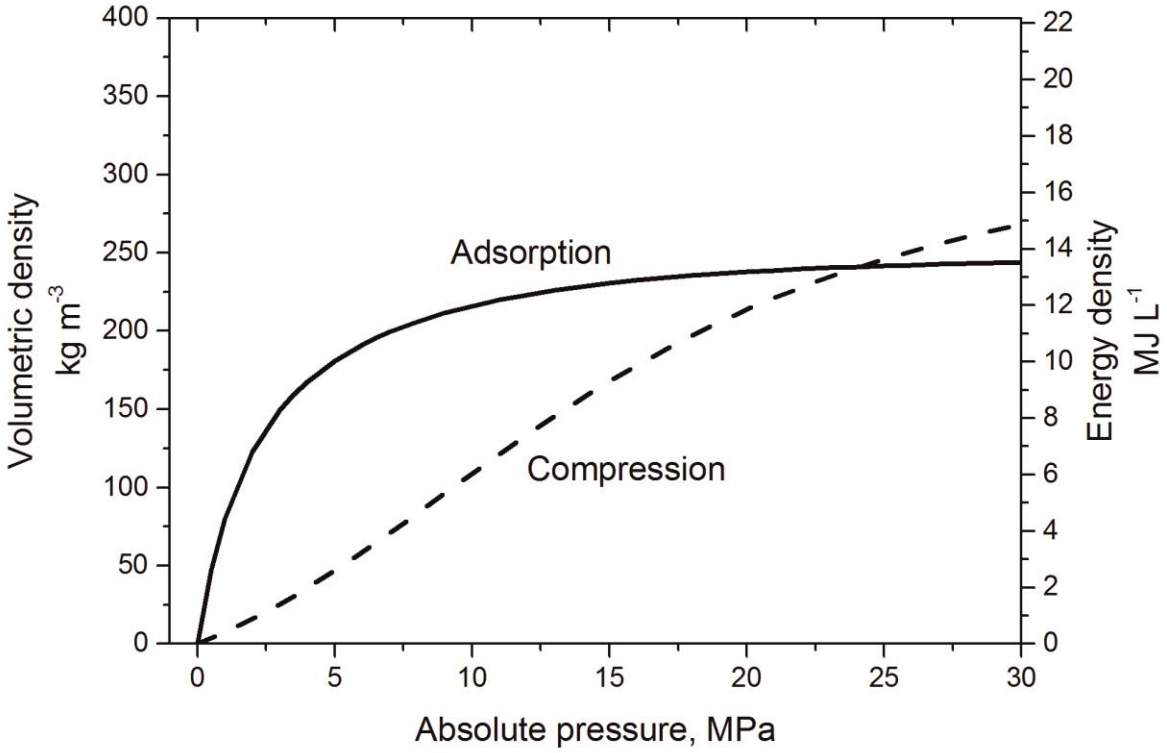
Volumetric density
kg m-3
Energy density
MJ L-1
Adsorption
Compression
Absolute pressure, MPa
0
50
100
150
200
250
300
350
400
0
2
4
6
8
10
12
14
16
18
20
22
0
5
10
15
20
25
30